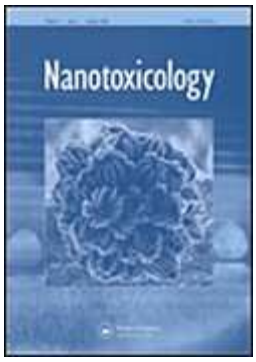

Investigation of the Cytotoxicity of Nanozeolites A and Y

Journal:	*Nanotoxicology*
Manuscript ID:	TNAN-2010-0227.R1
Manuscript Type:	Original Article
Date Submitted by the Author:	n/a
Complete List of Authors:	Thomassen, Leen; Katholieke Universiteit Leuven, Microbial and molecular systems Napierska, Dorota; Katholieke Universiteit Leuven, Laboratory of Lung Toxicology Dinsdale, David; MRC Toxicology Unit Lievens, Nele; Katholieke Universiteit Leuven, Microbial and molecular systems Jammaer, Jasper; Katholieke Universiteit Leuven, Microbial and molecular systems Lison, Dominique; Catholic University of Louvain, Industrial Toxicology and Occupational Medicine unit Kirschhock, Christine; Katholieke Universiteit Leuven, Microbial and molecular systems Hoet, Peter; KUleuven, Public Health Martens, Johan; KULeuven, Microbial and molecular systems
Keywords:	Nanotoxicology, Nanoparticles, Cytotoxicity, Zeolites, Aggregation

Investigation of the Cytotoxicity of Nanozeolites A and Y

LEEN C.J. THOMASSEN[1], DOROTA NAPIERSKA[2], DAVID DINSDALE[3], NELE LIEVENS[1], JASPER JAMMAER[1], DOMINIQUE LISON[3], CHRISTINE E.A. KIRSCHHOCK[1], PETER H. HOET[2] & JOHAN A. MARTENS[1*]

[1] Center for Surface Chemistry & Catalysis, Katholieke Universiteit Leuven, Kasteelpark Arenberg 23, 3001 Heverlee, Belgium, [2] Laboratory of Lung Toxicology, Katholieke Universiteit, Herestraat 49, 3000 Leuven, Belgium, [3] MRC Toxicology Unit, Lancaster Road, Leicester LE1 9HN, UK, [4] Louvain Centre for Toxicology and Applied Pharmacology, Université catholique de Louvain, Avenue E. Mounier, 53.02, 1200 Brussels, Belgium

L.C.J. Thomassen and D. Napierska contributed equally to this work.

Abstract

Nanosized zeolite particles are important materials for many applications in the field of nanotechnology. The possible adverse effects of these nanomaterials on human health have been scarcely investigated and remain largely unknown. This study reports the synthesis of nanozeolites Y and A with particle sizes of 25-100 nm and an adequate colloidal stability for *in vitro* cytotoxicity experiments. The cytotoxic response of macrophages, epithelial and endothelial cells to these nanocrystals was assessed by determining mitochondrial activity (MTT assay) and cell membrane integrity (LDH leakage assay). After 24h of exposure, no significant cytotoxic activity was detected for zeolite doses up to 500 µg/ml. Addition of fetal calf serum to the cell culture medium during exposure did not significantly change this low

response. The nanozeolites are of low toxicity compared with monodisperse amorphous silica nanoparticles of similar size (60 nm). These results may contribute to the application of nanozeolites for purposes such as medical imaging, sensing materials, low-*k* films and molecular separation processes.

Keywords: Zeolites, cytotoxicity, nanotoxicology, nanoparticles, aggregation

Correspondence: Prof. J.A. Martens, Center for Surface Chemistry & Catalysis, Katholieke Universiteit Leuven, Kasteelpark Arenberg 23, 3001 Heverlee, Belgium, fax: (+32) 16-321998, E-mail: johan.martens@biw.kuleuven.be

Introduction

Zeolites are crystalline microporous (alumino)-silicates with a tetrahedral framework. Theoretically infinite possibilities exist to connect framework tetrahedra by corner sharing. Today, 194 different zeolite structures with intracrystalline cages and channels of molecular dimensions are known. As crystalline materials, zeolites consist of a systematic repetition of unit cells in three dimensions, determining the cage and channel network in the crystal. To easily distinguish the different topologies, each has a unique three letter code (Baerlocher *et al.* 2007). For example, the framework structure of FAU (zeolite Y) consists of cuboctahedra linked to each other via double six rings enclosing large supercages, while in LTA (zeolite A), these cuboctahedra are linked via cubes. This results in very different pore sizes of about 8Å and 12Å, respectively.

Zeolite frameworks entirely built of [SiO_4] tetrahedra are electrically neutral, as the net composition equals SiO_2 and silicon assumes oxidation state IV. In an aluminosilicate zeolite, some [$Si^{IV}O_4$] tetrahedra are replaced by [$Al^{III}O_4$] units which introduce a negative charge into

the framework corresponding to the number of Al atoms. The negative charge of the framework is balanced with cations positioned inside of the zeolite cavities (Ghobarkar *et al.* 1999). The possibility of synthesizing the same topology with different Al-content allows the tailoring of the properties of the respective zeolite.

The high internal surface area caused by the open topology and the ion exchange capacity of zeolites induced by the presence of [AlO_4] tetrahedral, make zeolites unique materials for applications in catalysis, cation exchange, adsorption, and molecular sieving (Ghobarkar *et al.* 1999). These features can also be expected to play a role in interactions between zeolite crystals and cells.

The morphology of the crystals on the macroscale depends on the preferential growth direction of the crystal. For equal growth rates in 3 directions, a compact crystal is formed whereas elongated crystals or sheets grow preferentially in 1 or 2 directions.

Currently, the crystal size of commercial zeolites is in the micrometer range. Nano versions of many types of zeolites have also been synthesized (Tosheva and Valtchev 2005). These nanocrystals present potential benefits over their micron sized analogues due to their high surface area and short diffusion path lengths. The potential applications of nanozeolites are prominent in sensing materials, low-*k* films, molecular separation processes (Tosheva and Valtchev 2005), transfection of plasmid DNA (Pearce *et al.* 2008) and medical imaging (Tsotsalas *et al.* 2008, 2010; Ndiege *et al.* 2011). The growing commercialization of nano-products increases the potential for human exposure to nanoparticles, and many aspects related to the size of these materials have raised health and safety concerns. Several publications have highlighted the adverse effects of nanomaterials on the environment and human health (Oberdorster *et al.* 2005; Klaine *et al.* 2008; Stern and Mcneil 2008; Suh *et al.* 2009; Seaton *et*

al. 2010), including recent reviews on the toxicology of nanosized silica (Napierska *et al.* 2010; Petushkov *et al.* 2010b).

The toxicity of zeolites has been addressed in only few studies using natural or commercially available materials mainly in the micrometer size range. Adamis *et al.* (2000) investigated the toxicity of natural mordenite (MOR) and clinoptilolite (HEU) zeolites with crystal sizes smaller than 7 µm, both *in vitro* and *in vivo*. *In vitro* cytotoxicity was determined by measuring hemolysis of human red blood cells and LDH leakage from peritoneal rat macrophages after exposure to the zeolite samples. More than 95% hemolysis was observed after exposing human red blood cells for 1h to very high doses (2 mg/ml) of mordenite and clinoptilolite zeolites. On the other hand, incubation of peritoneal rat macrophages for 3 h with 300 µg zeolites /ml resulted in only moderate LDH release. *In vivo* experiments with intratracheal instillation of very high doses in rats (10-15 mg/rat) showed that clinoptilolite was innocuous, whereas mordenite induced acute and subacute inflammation. Those authors suggested that the higher *in vivo* toxicity of mordenite dust was due to the needle and rod-shaped particles in that particular sample. Another study performed with clinoptilolite, silicalite, KA, NaX and SAPO-11 zeolites, with HEU, MFI, LTA, FAU, and AEL topology reported a good stability of of the zeolites in simulated body fluid (Ceyhan *et al.* 2007). Low adverse effects (cell death < 5%) were reported after incubating chronic myelogeneous leukemia cells (5K562) and Swiss albino fibroblasts (3T3) with KA and silicalite zeolites (0.5-100 µM) for 3 days. The authors concluded that the zeolite treatment did not affect the cell division. Fenoglio *et al.* (2000a, 2000b) studied the cytotoxicity of micrometer sized synthetic pure-silica zeolites including faujasite, silicalite-1, ZSM-23 and theta-1 zeolites with FAU, MFI, MTT and TON topology, respectively. Cytotoxicity was measured after exposing proliferating J774 macrophages for 48 h. The cytotoxic effect of the porous zeolites was similar

to that of the natural dense crystalline silica polymorphs quartz, cristobalite, tridymite and coesite. A low response of 5 to 35% reduction in viability was recorded after exposing the cells to 5 µg/ml of zeolite. At the highest dose (50 µg/ml), nearly all cells were damaged by the faujasite, ZSM-23 and theta-1 zeolites, while silicalite-1 zeolites induced only about 25% cell death. The morphology of these crystals differed from isomeric crystals to elongated rod-shaped crystals. The authors concluded that elongated zeolite crystals were the most toxic and a positive correlation between the toxicity and the exposed zeolite surface area was established. Petushkov *et al.* (2009) investigated the cytotoxicity of three different silicalite-1 samples (MFI) with particle diameters of ca. 30, 150 and 500 nm on human embryonic kidney (HEK 293) and mouse monocyte macrophage (RAW 264.7) cell lines after 4h exposure. The bare 30 nm particles caused little effect on RAW264.7 but induced severe membrane damage in HEK293 cells, resulting in 35% cell death at a concentration of 1 mg/ml. The larger crystals caused up to 40% cytotoxicity in both cell lines at the highest concentrations tested (0.25 to 1 mg/ml). Tsotsalas *et al.* (2008, 2010) reported the synthesis and labeling of biocompatible zeolite L (LTL) nanoparticles with dye molecules and a radioactive tracer based on a earlier reported procedure (Li *et al.* 2006). A chemical 'stopcock' prevented labels from leakage to the physiological solution.

Nanozeolites have found to be stable against dissolution in phosphate buffered solutions at physiological pH and at 60°C for 24h (Petushkov *et al.* 2010a). Degradation of the (alumino)-silicate framework during *in vitro* experiments at 37°C is unlikely (Ceyhan *et al.* 2007).

Because of their unique pore structure, zeolite A and Y are popular industrial aluminosilicate materials (Vermeiren and Gilson 2009). It is likely that nanostructured zeolites will soon be used on a commercial scale. This study describes first the synthesis and characterization of nanosized zeolite Y (FAU type) and zeolite A (LTA type). Next, the *in vitro*

response of human lung epithelial cells, endothelial cells and macrophages upon exposure to these nanoparticles is reported.

Experimental

Synthesis of nanozeolites

Two different zeolite nanocrystals were synthesized. Zeolite Y was prepared according to the procedure of Holmberg *et al.* (2003). The molar composition of the synthesis mixture was 1 Al_2O_3 : 2.39 $(TMA)_2O$: 4.36 SiO_2 : 0.048 Na_2O : 249 H_2O. A 250 ml polypropylene bottle containing a magnetic stir bar was rinsed with deionized water. Then 74.82 g deionized water, 46.78 g TMAOH (25% in water, Acros) and 11.18 g aluminum isopropoxide (>98%, Acros) were added and stirred for 1 h at 400 rpm until a clear solution was obtained. An amount of 17.55 g of colloidal silica sol Ludox HS-40 (Sigma-Aldrich SiO_2/Na_2O = 0.95, Na_2O = 0.42 %), was added dropwise to the solution. The bottle was sealed and the mixture aged at room temperature for 3 days while stirring at 400 rpm. After this aging period, the mixture was heated to 100°C in an oil bath while stirring for 7 days.

The synthesis of zeolite A was based on a recipe by Mintova *et al.* (1999a). Although the synthesis procedure was described to yield zeolite Y, the obtained product had zeolite A crystal structure (LTA topology) containing some impurities with FAU topology. This is due to a high Na_2O/Al_2O_3 ratio in the synthesis mixture (Schoeman *et al.* 1994; Li *et al.* 2002). The starting mixture had a molar composition of 0.15 Na_2O : 5.5 $(TMA)_2O$: 2.3 Al_2O_3 : 10 SiO_2 : 570 H_20. The synthesis was carried out in a clean 250 ml polypropylene bottle containing a stirring bar. 4.70 g aluminum isopropoxide (Acros) and 0.06 g NaOH were dissolved in 40.72 g deionized water. Afterwards, 9.97g tetramethylammonium hydroxide pentahydrate (Acros) was

dissolved in the aqueous solution. Finally, 7.50 g of the colloidal silica sol (Ludox HS-40, Sigma-Aldrich), was added dropwise to the solution while stirring. The mixture was stirred at 400 rpm for 30 minutes and then heated to 100°C for 3 days while stirring continued.

Purification and sterilization

The as synthesized zeolite suspensions were purified from unreacted compounds of the synthesis mixture by dialysis. The suspensions were poured into a Nadir dialysis membrane (Carl Roth, pore diameter 2.5-3 nm) which was knotted on both ends. The membrane was placed in a 1-liter polypropylene vessel, filled with deionized water and placed on a rotating shaker. The agitation ensured a high concentration gradient over the dialysis membrane. The dialysate was refreshed 5 times over a total dialysis time span of 2 days.

The purified suspensions were filtered (PES membrane with pore diameter of 200 nm, Pall corp.) in order to remove possible microbial contamination. Nanozeolite powders were obtained by freeze drying 20 ml of purified suspensions in a ChristAlpha 1-2 apparatus. The samples were frozen in liquid nitrogen. Sublimation was done at a pressure of 0.2 kPa.

Prior to nitrogen sorption analysis, an organic template removal procedure from Holmberg *et al.* (2004) was applied on the nanozeolite samples. An amount of 0.3 wt% nanozeolite was stirred in a 1M $NaNO_3$ solution at 90°C for 16 h before purification by dialysis and freeze-drying.

Characterization of nanozeolites

X-Ray diffraction patterns were recorded in transmission mode on a STADI P diffractometer (STOE) with a CuKα source (λ=0.154 nm) and an image plate detector ($0 < 2\theta < 62°$). Patterns were recorded 20 times for 20 minutes and accumulated. TEM micrographs were obtained on a

Philips CM200 FEG instrument operated at 200 kV. Aqueous suspensions of nanozeolite Y and A were spread on a copper grid and allowed to dry in air overnight. Nitrogen sorption isotherms of the powder samples were recorded at -196°C using a TriStar apparatus (Micromeritics). Samples were pretreated at 250 °C under nitrogen flow during 12 h in a SmartPrep Programmable Degas System (Micromeritics). The total specific surface area was derived form the adsorption branch of the isotherms using the Brunauer-Emmett-Teller (BET) method (P/P_0 range 0.05-0.3) (Brunauer *et al.* 1938). The concentration of the samples was determined by analyses of the silicon content by ICP-AES (Perkin Elmer 4300 DV).

Zeta potential measurements were performed on a BIC ZetaPALS instrument (Brookhaven). The electrophoretic mobility was determined by phase analysis of the scattered laser light (658 nm, 30 mW) in forward scattering mode (angle 15°). The average and standard deviation of the zeta potential was calculated over 10 runs. The particle concentration for zeta potential measurements was 0.6 mg/ml. The pH of the aqueous suspension was adjusted with 0.01M NaOH until pH=9 and consequently lowered by addition of HCl (0.01-1 M) until pH=1 was reached. The zeta potential was measured at different acidities.

Stability of nanozeolites in cell culture medium

The stability of the suspensions was monitored in water and Dulbecco's Modified Eagle medium (DMEM, Invitrogen, Merelbeke, Belgium). Measurements of the hydrodynamic diameter in cell culture medium were performed immediately after suspending the particles in the media, and after subsequent incubation at 37°C for 24h. Dynamic light scattering (DLS) was performed in a BIC 90 Plus instrument (Brookhaven) equipped with 659 nm laser (15 mW) under a detection angle of 90°. The fluctuations in the scattered laser light intensity were correlated in 200 channels between 0.1 µs and 0.1s. Correlation functions were analyzed with

Igor Pro 6.02A using the Clementine package for modeling of Decay kinetics based on Maximum Entropy method. By converting the decay times with instrument parameters and Stokes-Einstein law to hydrodynamic diameters, an intensity weighted size distribution was obtained. Peak positions and widths were fitted with a lognormal function to obtain the average diameter of the particle populations.

In vitro cytotoxicity

In vitro cytotoxicity was assessed on three different cell lines: a human alveolar epithelial cell line (A549), a human endothelial cell line (EA.hy926, a permanent cell line established by Edgell *et al.* (1983)) and a human monocytic leukemia cell line (THP-1). The latter cell line was differentiated into macrophage like cells with phorbol myristate acetate (Alfaro-Moreno *et al.* 2008). At least two independent experiments were performed for each condition. In each experiment, the cytotoxic response to each condition was measured at least in triplicate. Dulbecco's modified eagle medium (DMEM), fetal calf serum (FCS), fungizone, L-glutamine (200 mM), penicillin–streptomycin (10000 U/mL and 10000 mg/mL, respectively), Dulbecco's phosphate buffered saline (DPBS) and Hank's balanced salt solution ($HBSS^{+}$) were obtained from Invitrogen (Merelbeke, Belgium). 3-(4,5-dimethylthiazol-2-yl)-2,5-diphenyltetrazolium bromide (MTT), dimethyl sulfoxide (DMSO), pyruvic acid, β-NADH and sodium bicarbonate were purchased from Sigma (Bornem, Belgium).

The human endothelial cells, epithelial cells and differentiated macrophages were seeded with cell densities of respectively 200,000, 150,000 and 200,000 cells/cm² in 96-well plates for cytotoxicity testing. The same cell densities were seeded in 24-well plates for quantification of cell-associated zeolites and cell imaging with optical microscope and in 12-well plates for

transmission electron microscopy investigations. The seeding medium was DMEM supplemented with 10% fetal calf serum (FCS), penicillin (100 U/ml), streptomycin (100 µg/ml), L-glutamine (2 mM) and fungizone (1.25 µg/ml). Cells were incubated at 37°C, 5% CO_2 and 100% humidity in an autoflow CO_2 jacked incubator (NUAIR). After 24 h, confluent cells were washed twice with DMEM- (without FCS or antibiotics) and subsequently incubated for 24 h in 200 µl DMEM containing nanozeolites at concentrations of 25, 50, 100, 250, 500, 1000 and 2000 µg/ml in the absence of FCS and supplements (DMEM-) or in presence of 2% heat inactivated FCS (DMEM+). The nanoparticle dispersions in DMEM- and DMEM+ were prepared immediately before use by serial dilution of the stock suspension followed by intense vortexing. Controls were incubated in an equivalent volume of DMEM- and DMEM+.

At the end of the exposure period, the cytotoxic response was evaluated on the one hand with tetrazolium reduction (MTT) assay which measures the respiratory mitochondrial activity of the cells (Loveland *et al.* 1992; Hillegass *et al.* 2010; Stone *et al.* 2009). On the other hand, lactate dehydrogenase (LDH)-leakage determination was applied as an indicator of membrane damage resulting from late apoptosis or necrosis (Hillegass *et al.* 2010; Stone *et al.* 2009). Monodisperse amorphous silica nanoparticles of 60 nm in diameter with a BET surface area of 42 m^2/g were used as a positive control in experiments performed in absence of FCS. The synthesis, characterization and toxicological effects of these nanoparticles were reported in previous publications (Napierska *et al.* 2009; Thomassen *et al.* 2010; Gonzalez *et al.* 2010; Rabolli *et al.* 2010). The EC_{50} values of the cells exposed to the monodisperse amorphous silica were calculated using the ED50plus v1.0 software.

In order to quantify the LDH activity in the samples, 50 µl of the supernatant of the cells was mixed with 100 µl DPBS and 100 µl of the measurement solution (1mM NADH, 5mM

pyruvate and 10 mM sodiumbicarbonate in DPBS). The maximal LDH release was determined by lysing control cells in 200 µl of a 0.2% Triton-X-100 solution in DPBS. The LDH activity was determined as described earlier (Napierska *et al.* 2009). Results are presented as a percentage of the control values.

The MTT assay determines the mitochondrial activity of the cells. After 24 h exposure to nanoparticles, cells were washed twice with $HBSS^+$ and incubated for 3 h at 37°C with 200 µl of the MTT solution (0.5 mg MTT/ml $HBSS^+$). The formazan product was dissolved in 100 µl DMSO after discarding the MTT solution. The absorbance was recorded with a microplate reader (Bio-Rad, Benchmark) at 550 nm and with a reference beam at 655 nm. The response in the treated group was expressed as a percentage of non-treated control group, which was assumed to be 100%.

To exclude false-positive results due to catalytic activity of the particles, the nanozeolites were incubated in absence of cells with MTT solution and LDH reaction mixture, respectively. The nanozeolites were found to be catalytically inactive in these test conditions. To investigate the interaction of nanozeolites with LDH enzymes, particles were incubated with control cell lysate. Measurement of LDH after the incubation indicated that the nanozeolites did not interfere with the assay by irreversible adsorption or denaturation of LDH enzyme. *Statistical analysis.* Data are presented as mean from two or three independent experiments with standard deviation (SD). Each experimental value was compared to the corresponding control value. Statistical analyses were performed by one-way analysis of variance followed by Dunnett post hoc test. Differences among means were considered significant with $*p<0.05$, and $**p<0.01$ for responses to nanozeolite Y and $^{\#}p<0.05$, and $^{\#\#}p<0.01$ for responses to nanozeolite A.

Cellular morphology and uptake

After incubation for 24 h with 0, 500 and 2000 µg/ml nanozeolites in 24-well plates, digital images of the cells were taken using an inverted light microscope CK2 Olympus (Japan). Subsequently, the cells were washed three times with 1ml $HBSS^{+}$ per well to remove nanozeolites which were not associated with the cells. The remaining zeolites and cells were dissolved in 1M NaOH. The samples were diluted 10x before analysis of the silica content by ICP-AES (Perkin Elmer 4300 DV). Each condition was measured in triplicate.

In a parallel experiment, all three cell-types were grown in 12 well plates, incubated for 24 h with 250 µg/ml nanozeolites A or Y, in the presence or absence of FCS. They were then fixed with 2% glutaraldehyde (EM grade) in 0.1M sodium cacodylate, final pH 7.2, at 37° C for 3h and removed from the substrate with a cell scraper. The cells were then pelleted by centrifugation (10 min at 300 rpm) and stored in the fixation buffer. The pellets were postfixed with 1% osmium tetroxide/1% potassium ferrocyanide for 1 h at room temperature. After fixation, cells were treated with 5% aqueous uranyl acetate overnight at room temperature, dehydrated, and embedded in Taab epoxy resin (Taab Laboratories Equipment Ltd., Aldermaston, UK). Electron micrographs of unstained, ultrathin sections were recorded using an ES1000W CCD camera and DigitalMicrograph software (Gatan, Abingdon, UK) in a Zeiss 902A electron microscope. For reference measurements, aqueous suspensions of each zeolite were passed through HA membrane filters (Millipore), these filters were also dehydrated, embedded and sectioned for electron microscopy.

Results

Characterization of synthesized nanozeolites

Nanozeolites were synthesized following the procedures of Holmberg *et al.* (2003) and Mintova *et al.* (1999a). The samples were purified by dialysis. The size and morphology of the particles in the purified suspensions were investigated by TEM (Figure 1). The TEM pictures revealed nanoparticles with well defined crystal planes. Cubic and rhombohedral crystal shapes were dominant. The edges of nanozeolite Y measured 25 to 50 nm (Figure 1A). Zeolite A had larger crystal dimensions with crystal edges from 45 to 100 nm (Figure1B).

[Insert Figure 1 about here]

The bottom panels in Figure 1 at the highest magnification visualize lattice fringes confirming the crystallinity of the particles. The lattice spacing of 14 Å in zeolite Y was attributed to the (111) planes of the FAU structure (Mintova *et al.* 1999b). A characteristic lattice spacing of 12.3Å was observed for zeolite A (Cruz *et al.* 1978).

XRD patterns of the freeze-dried nanozeolite samples and reference micron size zeolite samples are shown in Figure 2.

[Insert Figure 2 about here]

The XRD patterns of the nanozeolites presented a superposition of broadened Bragg reflections on very broad background features (Figure 2). The diffraction angles of the peaks in the XRD pattern of nanozeolite Y sample corresponded to the main diffractions of micron size zeolite Y reference powder (Figure 2a&b). The XRD pattern of the nanozeolite Y could be indexed in the correct cubic F-3d spacegroup with unit cell size of 24.83 Å, characteristic of a FAU type zeolite. The substantial broadening of the diffraction peaks of the nanozeolite compared to the micron size reference is due to the nanometer dimensions of the crystals. The presence of the broad background may be related to the presence of some amorphous or less

ordered domains in the sample. The Bragg reflections of nanozeolite A correspond to those of reference zeolite A material with LTA topology (Figure 2c&d). The diffraction around 6° 2θ might be due to minor traces of FAU type zeolite in this sample.

Nitrogen adsorption isotherms of the nanocrystals are displayed in Figure 3. The samples showed strong nitrogen adsorption at very low relative pressures owing to micropore filling and an upswing of the isotherms at higher pressures due to multilayer adsorption on the large external surface area exposed by these nanoparticles. The nitrogen uptake in zeolite A (Figure 3b) at low pressures was substantially lower than in zeolite Y (Figure 3a). In zeolite A at -196°C the access of the supercages to nitrogen molecules is hampered by the positioning of Na^+ cations in the 8-membered ring windows giving access to the cages. Therefore, zeolite A does not show pronounced uptake of nitrogen molecules at the boiling point of liquid nitrogen.

[Insert Figure 3 about here]

The BET specific surface area of nanozeolite Y was ca. 375 m²/g, which is close to the value of 449 m²/g reported by Holmberg *et al.* (2004). It should be noted that those authors applied a slightly different synthesis procedure and purification which may account for the discrepancy in the specific surface area. The specific surface area of the nanozeolite A was ca. 241 m²/g and should mainly reflect external surface area.

The interactions between zeolite crystals in a suspension can be described by the DLVO theory (Deraguin-Landau-Verwey-Overbeek), which takes into account van der Waals forces as well as repulsion, caused by the overlap of the electric double layer of the particles (Nikolakis 2005). The zeta potential, describing the surface charge of the particles, is a measure for the electrostatic repulsion between particles, and can be used as an indicator for dispersion stability (Kuzniatsova *et al.* 2007; Brinker and Scherer 1990). The surface charge of zeolites results

from the dissociation of the hydroxyl groups, so that the pH controls the zeta potential through the following mechanisms:

$(T\text{-}O\text{-})_3Si\text{-}OH + OH^- \leftrightarrow (T\text{-}O\text{-})_3Si\text{-}O^- + H_2O$

$(T\text{-}O\text{-})_3Si\text{-}HO^{\cdots}Al(\text{-}O\text{-}Si)_3 + OH^- \leftrightarrow (T\text{-}O\text{-})_3Si\text{-}O\text{-}Al^-(\text{-}O\text{-}Si)_3 + H_2O$, with T symbolising a framework atom.

Hence, the zeta potential of zeolites at a given pH depends on the number of surface hydroxyls which is determined by framework composition, zeolite topology and particle morphology (Maurer *et al.* 2001; Kuzniatsova *et al.* 2007). Ionic strength of the medium and the aluminum content of the framework have impact on the zeta potential. While increasing ion content contributes to shielding of surface charge, increasing numbers of framework aluminum increases the negative surface charge, lowering the zeta potentials of alumosilica zeolites and shifting the isoelectric point towards lower pH (Nikolakis 2005; Caro *et al.* 2009; Kuzniatsova *et al.* 2007). This phenomenon is attributed to the high acidicy of protonated $(T\text{-}O)_3Si\text{-}O\text{-}Al^-(Si\text{-}O)_3$ bridges on the surface, which are only neutralised at high proton concentrations (Maurer *et al.* 2001).

Figure 4 shows the zeta potential of the particles determined in water at different pH values. The zeta potential and thus the surface charge of the particles became more negative with increasing pH of the nanozeolite environment. At increasing pH values, deprotonation of silanol groups is resulting in increasing numbers of negatively charged sites at the particle surface. At neutral pH (pH 7) the zeta potential of the particles was strongly negative (ca. -40 mV). The iso-electric point (IEP) of the nanozeolites was reached around pH 3-4. At this pH the particles agglomerated and precipitated rapidly and reversibly.

[Insert Figure 4 about here]

Stability of nanozeolites in cell culture medium

The hydrodynamic diameter of the nanocrystals in deionized water and in DMEM- (3 µg/ml) was determined using DLS. The intensity weighed average hydrodynamic particle size of nanozeolite Y and A in water was 120 nm and 151 nm, respectively. A larger hydrodynamic diameter compared to the number weighed diameter according to TEM was to be expected (Thomassen *et al.* 2010). Upon suspending the particles in DMEM-, a slight increase in average hydrodynamic diameter to 140 and 159 nm for zeolite Y and A, respectively, was observed. This may be due to a larger hydration layer around multivalent ions, present in the DMEM medium and associated with the silica surface (Thomassen *et al.* 2010). DLS revealed no significant changes in hydrodynamic particle diameter at 3 µg/ml nanozeolites in DMEM upon 24 h incubation at 37°C.

The stability of the suspensions with particle concentrations of 25 µg/ml, corresponding to the lowest concentrations used in toxicological experiments, in standard medium (DMEM-) or in medium supplemented with 2% fetal calf serum (DMEM+), were also monitored by DLS (Figure 5). Upon suspending the particles in DMEM (Figure 5, full lines), the particle size was similar to the particle sizes measured at low (3 µg/ml) particle concentration in water and DMEM-. The addition of FCS had a stabilizing effect on the particle suspensions, monitored by a slight reduction in average particle size (Figure 5C&D, full lines) compared to the particle suspensions in DMEM without FCS (Figure 5A&B, full lines). After storage over 24 h at 37°C, two distinct particle size populations were observed in the DMEM- suspensions (Figure 5A&B, dotted line). Primary nanozeolites (ca. 40 nm) were detected next to larger aggregates. The average hydrodynamic diameter of the suspensions in DMEM+ did not change during the time

frame of the toxicological tests. DLS measurements of higher particle concentrations (50 and 100 µg/ml) yielded similar results. DLS is applicable only to suspensions with a low particle concentration. Measurements in concentrated suspensions are biased by multiple scattering. Therefore, it was not possible to measure the size of the particles in suspension at the highest doses (250 – 2000 µg/ml) used in the cytotoxicity testing.

[Insert Figure 5 about here]

In DMEM-, the zeta potential of nanozeolite Y and nanozeolite A were -16 and -23 mV, respectively. The cations present in the DMEM medium interact with the negative particle surface and made the zeta potential less negative compared to the zeta potential in water at physiological pH (Figure 4). This explains the limited stability of the particle suspension in DMEM. Precipitation or gelation of nanozeolites was never observed, even at concentrations as high as 2 mg/ml. In DMEM+ the zeta potential is even less negative with values of -10 and -14 mV for nanozeolite Y and nanozeolite A respectively. The suspensions were more stable in DMEM+ over the 24h exposure time frame despite lower electrostatic repulsion forces in the nanozeolite suspensions suspended in DMEM+ compared to DMEM-. This increased stability can be induced by steric repulsion forces created by adsorbed proteins on the nanozeolite surfaces.

Determination of the nanozeolite cytotoxic activity

The cytotoxic activity of these nanozeolites was investigated on three different cell lines: (i) alveolar epithelial cells (A549), (ii) human endothelial cells (EA.hy926) and (iii) differentiated macrophages (THP-1). The cells were exposed for 24h to nanozeolite concentrations from 25 up to 2000 µg/ml in cell culture medium without (DMEM-) and with addition of 2% FCS (DMEM+). The same exposure protocol was used to asses the toxicity of the positive control, a

stable suspension of 60 nm monodisperse amorphous nanoparticles in DMEM-. The cytotoxicity of the amorphous nanoparticles against endothelial cells was reported by Napierska *et al.* (2009). The effect of the nanozeolites and amorphous silica nanoparticles on the cells was assessed by two independent methods, viz. the MTT assay and LDH leakage measurements. Two different cytotoxicity assays were used to be able to detect possible interference of the test material with the assay (Worle-Knirsch *et al.* 2006; Stone *et al.* 2009).

In the MTT assay the mitochondrial activity of the exposed cells was assessed and compared to control cells. For particles suspended in DMEM- (Figure 6, left panel), a significantly decreased mitochondrial activity of epithelial cells was observed only at the highest dose (2 mg/ml) for both nanozeolites. This high nanozeolites concentration reduced the viability of A549 cells with only 15%. Exposure to 250 and 500 µg/ml of nanozeolite Y caused significantly higher mitochondrial activity in the epithelial cells, suggesting an activation of the cells. For macrophages, significantly lower mitochondrial activity was measured only after exposure to high concentrations of nanozeolite Y (1 and 2 mg/ml), and nanozeolite A (≥500 µg/ml). Endothelial cells showed the highest sensitivity to nanozeolite A with significantly reduced mitochondrial activity after incubation with at least 250 µg/ml of this particle. The response of EA.hy926 cells to nanozeolite Y was only significant after exposure to 1 or 2 mg/ml of nanozeolite Y. The monodisperse amorphous silica in DMEM- was more toxic than the nanozeolites towards all cell lines since the latter barely show toxicity at mass concentrations which cause 50% cell death by the amorphous silica (diamonds in Figure 6, left panel).

The presence of FCS during exposure to the nanozeolites (Figure 6, right panel) showed only a few different responses (however, no higher cytotoxicity) in tested epithelial and

endothelial cells using MTT assay. Nanozeolite Y did not cause any cell activation in epithelial cells and decreased significantly the mitochondrial activity above 1 mg/ml. Nanozeolite A showed significantly higher toxic effect towards A549 cells only at concentration of 500 µg/ml. Addition of 2% FCS into the cell culture medium of endothelial cells caused less cytotoxic response to nanozeolite Y when compared to test performed without FCS; however, the measured mitochondrial activity was significantly lower at concentrations above 500 µg/ml when compared to control values. The most pronounced differences in the results of MTT assays were observed in macrophages. Exposure to nanozeolite A did not cause any significant toxicity at any concentration tested, and the macrophages showed significantly higher mitochondrial activity in broad range of concentrations (100-1000 µg/ml). Addition of 2% FCS into the cell culture medium of macrophages did cause less cytotoxic response to nanozeolite Y when compared to tests performed without FCS.

[Insert Figure 6 about here]

Membrane damage was assessed by measurement of LDH leakage from the cells. For the three cell lines, no LDH leakage was observed after 24h exposure to nanozeolite Y or A in DMEM- nor in DMEM+ (Figure 6, right columns of each panel). The monodisperse amorphous silica caused cell death in 50% of exposed cells at concentrations of about 100 µg/ml in A549 and THP-1 cells while EA.hy926 cells were more resistant to the silica nanoparticles. The cytotoxic responses to the positive control measured by MTT and LDH assay were similar.

Morphological changes in the cells were investigated under a light microscope after exposure to 500 µg/ml and 2000 µg/ml of nanozeolite Y in DMEM- (Figure 7). The endothelial and epithelial cells formed a confluent layer in the control wells. After exposure to 500 µg/ml

nanozeolite Y, some morphological changes were noticed. The epithelial and endothelial cell culture became less confluent and some cells adopted a spherical cell shape. After 24 h exposure to the highest concentration, the density of epithelial cells was reduced. Endothelial cells had dramatically changed morphology and all adopted a round cell shape. Macrophages appeared to have a rougher surface after exposure to nanoparticles. Similar observations were made after exposing the cells to nanozeolite A and in the presence of FCS (data not shown).

[Insert Figure 7 about here]

The presence of cell-associated nanozeolites was confirmed by ICP-AES measurements (Table 1). After exposing the cells to 500 µg/ml nanozeolites, about 30 to 50% of the zeolites were strongly associated with the cells since they were not removed after three rinsing steps.

[Insert Table I about here]

ICP-AES measurements quantify the total amount of nanozeolites associated with the cells. However the question whether the particles are taken up by the cells cannot be solved by these measurements since it is not possible to discriminate between nanozeolites adsorbed on the cell surface and internalized nanozeolites. Particles of nanozeolites A and Y were clearly visible by electron microscopy in unstained sections of membrane filters but surprisingly few were found in the cell pellets. Any particles present in these pellets were restricted to cytoplasmic vacuoles in THP-1 cells (Figure 8A). The majority of THP-1 cells, exposed to either zeolite, contained many vacuoles (Figure 8B). In contrast, exposure of A549 and EA.hy926 cells to the nanozeolites resulted in only a slight augmentation of the normal multivesicular and lamellar bodies but otherwise the cells appeared to be unaffected (Figure 8 C&D). Incorporation of FCS into the culture medium had no discernible effect on these results.

[Insert Figure 8 about here]

Discussion

Potential physicochemical determinants of nanoparticle toxicology are size, crystallinity, surface morphology, surface functionalization and charge (Oberdorster *et al.* 2005). A good physicochemical characterization of nanoparticles is mandatory before conducting any toxicological assays (Warheit 2008; Seaton *et al.* 2010). The extensive characterization of zeolite Y and A by means of TEM, XRD, nitrogen sorption confirmed the successful synthesis of cubic zeolite crystals with FAU and LTA topology in the range of 25-50 and 45-100 nm, respectively. Zeta potential analysis and DLS measurements in the cell culture medium, showed that the nanozeolites were sufficiently stable under these conditions.

The cytotoxic activity of synthesized nanozeolites Y and A was assessed. A low toxic response was measured with the MTT and LDH assay for all cell lines and both nanozeolites tested in DMEM medium with or without addition of FCS (Figure 6). For the highest doses (1 and 2 mg/ml) the viability measured by the MTT method is diverging from the results obtained by the LDH assay. The cell morphology and culture density alterations, revealed by light microscopy (Figure 7), were consistent with the cytotoxic responses detected by the MTT method. The discrepancy between the MTT and LDH assay measured at high nanozeolite concentrations may be due to a delay between the termination of respiratory function and cell membrane rupture. By measuring LDH activity after incubating LDH enzyme from lysed cells with nanozeolites in an acellular environment, irreversible adsorption or denaturation of LDH enzyme due to interaction with nanoparticles was excluded (data not shown). High concentrations of cell-associated zeolites were confirmed by ICP-AES analysis of the cells after three rinsing steps (Table 1). Since the nanozeolites did not gelate in the acellular cell culture medium (Figure 4), this high dose of cell-associated zeolites is probably due to an

interaction of zeolites with cellular components. Nevertheless, we did not find any evidence of particles on the surface of cells examined by electron microscopy. This absence may well have resulted from the numerous washes involved in the processing of these samples. A higher affinity of the nanozeolites for the chemicals applied in the EM preparation process compared to the PBS rinsing buffer applied in the preparation for ICP-AES measurements can explain the apparent absence of adsorbed nanozeolites on cells examined by EM.

Low cytotoxic responses are consistent with the absence of particles, detectable by EM, in either A549 or EA.hy926 cells. The presence of a few particles in the THP-1 cells is consistent with the phagocytic activity of these cells. Addition of FCS in the cell culture media during exposure to the particles, did not increase particle uptake by any cell type.

Nanozeolites Y and A induced a lower cytotoxic response than pure amorphous silica particles of similar size in the epithelial, endothelial and macrophage cells. Although micrometer sized zeolites are generally more toxic than micrometer sized amorphous silica (Fenoglio *et al.* 2000b; André Pierre Legrand *et al.* 1998), this does not appear to be the case when the particle size is lowered to the nanoscale.

The low toxicity of nanozeolites Y and A is consistent with the low toxicity of pure silica nanozeolites (MFI) on a macrophage cell line (Petushkov *et al.* 2009). In addition, aluminosilicates like zeolite A and Y may exhibit a lower hazard than pure silica zeolites. Fenoglio *et al.* (2000a, 2000b) reported that quartz and pure silica zeolites treated with aluminum lactate exhibited a lower cytotoxicity than the original samples. Each substitution of silicon atom by an aluminum atom generates a negative charge. Therefore, an aluminosilicate has a more negative charge in neutral solution than pure silica, reducing the

adsorption of organic molecules by hydrogen bonding. This may explain why an aluminosilicate surface is less harmful to the cell than a pure silica surface (Iler 1981).

In literature, the importance of measuring the total surface area (BET) is indicated (Fubini *et al.* 2010; Singh *et al.* 2007). The cellular response is often correlated to the large surface area of nanoparticles exposed to cells (Rabolli *et al.* 2010; Singh *et al.* 2007; Stoeger et al. 2009; Oberdörster et al. 2000; Auffan et al. 2009). On the other hand, Lanone et al. (2009) did not find any correlation between cytotoxicity and BET surface area after evaluating the cytotoxic effect of 24 nanoparticles with various elemental compositions on 2 human cell lines.

In these experiments, the large BET surface area of nanozeolite Y and A (resp. 375 and 241 m^2/g) does not induce severe cellular responses. It is important to mention that the total surface area (BET) consists of the external and internal surface area of the crystals. According to Fenoglio *et al.* (2000a) the internal surface of zeolites is not involved in the mechanisms of cytotoxicity. Similar findings were reported for mesoporous silica nanoparticles by Slowing *et al.* (2009). These authors demonstrated that the hemolytic properties of these particles are related to the number of silanol groups accessible to the cell membranes. The internal surface was not involved in the observed toxicity towards red blood cells. In addition, microporous amorphous silica nanoparticles (74 nm) were significantly less cytotoxic towards endothelial cells than the 60 nm silica nanoparticles used as positive control in the present study (Napierska *et al.* 2009).

Conclusions

Suspensions of nanozeolites Y and A were prepared with particle sizes of 25-50 nm and 45-100 nm, respectively. The colloidal suspensions were sufficiently stable in physiologic medium. The low zeta potential of the particles at neutral pH (<-40 mV) contributes to the stability of the suspension. The nanozeolite suspensions were stable for 24 h in the DMEM cell culture medium with high ionic strength at low particle concentrations (3 µg/ml). At higher concentrations, aggregates were observed next to primary particles. Addition of 2% FCS to the cell culture medium increased the stability of the particle suspensions, so that no aggregates were observed after 24h of incubation time.

Cytotoxicological experiments using human alveolar epithelial cells (A549), human endothelial cells (EA.hy926) and differentiated monocytes (THP-1) revealed a slightly decreased mitochondrial activity only at extremely high nanoparticle concentrations of 1 and 2 mg/ml in DMEM with and without FCS. The LDH assay did not show a loss in membrane integrity at these concentrations. After exposure to 500 µg/ml nanozeolites, up to 50% of the administered nanoparticle mass was found to be associated with the cells. However only few nanozeolites were internalized in macrophage cells. There was no evidence for uptake in endothelial and epithelial cells. These zeolite nanoparticles induced very low *in vitro* toxicity compared to the positive control of similar size (60 nm amorphous silica nanoparticles), despite an approximately 10-fold greater specific surface area. This might suggest that for microporous particles, the internal surface does not contribute to the biological activity of the particles. The low cytotoxic activity of nanozeolites will contribute to promote the future industrial and medical applications of these particles.

Acknowledgements

This work was supported by the Belgian Science Policy program "Science for a Sustainable Development" (SD/HE/02A). JAM acknowledges the Flemish Government for long-term structural funding (Methusalem). The authors are grateful to Judy McWilliam and Tim Smith for the preparation of material for EM.

Competing financial interests.

None

Table

Table I: Percentage cell-associated nanozeolites after exposure for 24h to 500 µg/ml nanozeolites in DMEM-

	Zeolite Y	Zeolite A
A549	30 %	45 %
EA.hy926	33 %	45 %
THP-1	34 %	49 %

Figure captions

Figure 1: TEM pictures of zeolite Y (column A) and zeolite A (column B) reveal size, morphology and lattice fringes of the nanocrystals.

Figure 2: XRD pattern of nanozeolite Y (a), micron size zeolite Y (b), nanozeolite A (c) and micron size zeolite A (d). XRD patterns of micron size zeolites are duplicated from Baerlocher *et al.* (2007).

Figure 3: Nitrogen sorption isotherm of zeolite Y (a) and zeolite A (b). The ad- and desorption branches are in full and dotted lines, respectively.

Figure 4: Zeta potential of nanozeolite Y (squares) and nanozeolite A (triangles) in water as a function of pH.

Figure 5: Evolution of hydrodynamic diameter of 25 µg/ml nanozeolites after 0 h (full line) and 24 h (dotted line) incubation in cell culture medium: (A) zeolite Y in DMEM-, (B) zeolite A in DMEM-, (C) zeolite Y in DMEM+, (D) zeolite A in DMEM+.

Figure 6: Dose-effect relationships in epithelial cells (A549, top), endothelial cells (EA.hy926, middle) and macrophages (THP-1, bottom) after 24 h exposure to the zeolite Y (full squares) and zeolite A (open circles) nanocrystals. Cells were exposed to nanozeolites in DMEM in absence of FCS (DMEM-: left pane) or presence of 2% FCS (DMEM+: right panel). Viability was assessed with MTT test (left column) and LDH leakage determination (right column) and results are presented as a percentage of the control values (average ± SD, $n \geq 6$). The EC_{50} of the positive control, amorphous silica of 60 nm, in DMEM- is displayed in each graph by a diamond marker. Differences among means were considered significant with *$p<0.05$, and **$p<0.01$ for responses to nanozeolite Y and $^{\#}p<0.05$, and $^{\#\#}p<0.01$ for responses to nanozeolite A.

Figure 7: Light microscopy images of control cells and cells exposed to 500 µg/ml and 2000 µg/ml of zeolite Y after 24h exposure in DMEM-.

Figure 8: Electron micrographs of cells exposed to 250 µg/ml zeolites for 24 h. (A) A few particles of zeolite Y (black arrows) are evident within a vacuole of a THP-1 cell exposed in the absence of FCS. (B) Similar vacuoles (black arrows) are present in THP-1 cells exposed to this zeolite in the presence of FCS. (C) A549 cells exhibit very few vacuoles but, like controls, numerous lamellar bodies (white arrows) are present. (D) EA.hy926 cells resemble controls, with several lamellar bodies (white arrows) and multivesicular bodies (white arrowheads). Scale bars = 1µm.

References

Adamis Z, Tatrai E, Honma K, Six E, Ungvary G. 2000. In vitro and in vivo tests for determination of the pathogenicity of quartz, diatomaceous earth, mordenite and clinoptilolite. Annals of Occupational Hygiene 44:67-74.

Alfaro-Moreno E, Nawrot TS, Vanaudenaerde BM, Hoylaerts MF, Vanoirbeek JA, Nemery B, Hoet PHM. 2008. Co-cultures of multiple cell types mimic pulmonary cell communication in response to urban PM10. European Respiratory Journal 32:1184-1194.

Auffan M, Rose J, Orsiere T, De Meo M, Thill A, Zeyons O, Proux O, Masion A, Chaurand P, Spalla O et al. 2009. CeO2 nanoparticles induce DNA damage towards human dermal fibroblasts in vitro. Nanotoxicology 3:161-U115.

Baerlocher C, McCusker LB, Olson DH. 2007. In: Atlas of zeolite framework types. 6 ed. Amsterdam: Elsevier.

Brinker CJ, Scherer GW. 1990. In: Sol-Gel Science: The Physics and Chemistry of Sol-Gel Processing 2nd ed. London: Academic Press.

Brunauer S, Emmett PH, Teller E. 1938. Adsorption of gases in multimolecular layers. Journal of the American Chemical Society 60:309-319.

Caro J, Albrecht D, Noack M. 2009. Why is it so extremely difficult to prepare shape-selective Al-rich zeolite membranes like LTA and FAU for gas separation? Separation and Purification Technology 66:143-147.

Ceyhan T, Tatlier M, Akcakaya H. 2007. In vitro evaluation of the use of zeolites as biomaterials: effects on simulated body fluid and two types of cells. Journal of Materials Science-Materials in Medicine 18:1557-1562.

Cruz WV, Leung PCW, Seff K. 1978. Crystal-Structures of Cyclopropane Complexes of Cobalt(Ii) and Manganese(Ii) in Partially Exchanged Zeolite-A. Journal of the American Chemical Society 100:6997-7003.

Edgell CJ, Mcdonald CC, Graham JB. 1983. Permanent Cell-Line Expressing Human Factor-Viii-Related Antigen Established by Hybridization. Proceedings of the National Academy of Sciences of the United States of America-Biological Sciences 80:3734-3737.

Fenoglio I, Croce A, Di Renzo F, Tiozzo R, Fubini B. 2000a. Pure-silica zeolites (porosils) as model solids for the evaluation of the physicochemical features determining silica toxicity to macrophages. Chemical Research in Toxicology 13:489-500.

Fenoglio I, Fubini B, Tiozzo R, Di Renzo F. 2000b. Effect of micromorphology and surface reactivity of several unusual forms of crystalline silica on the toxicity to a monocyte-macrophage tumor cell line. Inhalation Toxicology 12:81-89.

Fubini, B. 1998. Health Effects of Silica. In: André P.Legrand, editor. The Surface Properties of Silicas. West Sussex: John Wiley & Sons. pp 415-465.

Fubini B, Ghiazza M, Fenoglio I. 2010. Physico-chemical features of engineered nanoparticles relevant to their toxicity. Nanotoxicology 4:347-363.

Ghobarkar H, Schaf O, Guth U. 1999. Zeolites - from kitchen to space. Progress in Solid State Chemistry 27:29-73.

Gonzalez L, Thomassen LCJ, Plas G, Rabolli V, Napierska D, Decordier I, Roelants M, Hoet PH, Kirschhock CEA, Martens JA *et al.* 2010. Exploring the aneugenic and clastogenic potential in the nanosize range: A549 human lung carcinoma cells and amorphous monodisperse silica nanoparticles as models. Nanotoxicology 4:382-395.

Hillegass JM, Shukla A, Lathrop SA, MacPherson MB, Fukagawa NK, Mossman BT. 2010. Assessing nanotoxicity in cells in vitro. Wiley Interdisciplinary Reviews-Nanomedicine and Nanobiotechnology 2:219-231.

Holmberg BA, Wang HT, Norbeck JM, Yan YS. 2003. Controlling size and yield of zeolite Y nanocrystals using tetramethylammonium bromide. Microporous and Mesoporous Materials 59:13-28.

Holmberg BA, Wang H, Yan YS. 2004. High silica zeolite Y nanocrystals by dealumination and direct synthesis. Microporous and Mesoporous Materials 74:189-198.

Iler, RK 1981. The surface chemistry of amorphous synthetic silica: Interaction with organic molecules in an aqueous medium. In: Dunnom DD editor. Health effects of synthetic silica particulates: Philadelphia: American Society for Testing and Materials. pp. 3-21.

Klaine SJ, Alvarez PJJ, Batley GE, Fernandes TF, Handy RD, Lyon DY, Mahendra S, McLaughlin MJ, Lead JR. 2008. Nanomaterials in the environment: Behavior, fate, bioavailability, and effects. Environmental Toxicology and Chemistry 27:1825-1851.

Kuzniatsova T, Kim Y, Shqau K, Dutta PK, Verweij H. 2007. Zeta potential measurements of zeolite Y: Application in homogeneous deposition of particle coatings. Microporous and Mesoporous Materials 103:102-107.

Li QH, Creaser D, Sterte J. 2002. An investigation of the nucleation/crystallization kinetics of nanosized colloidal faujasite zeolites. Chemistry of Materials 14:1319-1324.

Li HR, Devaux A, Popovic Z, De Cola L, Calzaferri G. 2006. Carboxyester functionalised dye-zeolite L host-guest materials. Microporous and Mesoporous Materials 95:112-117.

Loveland BE, Johns TG, Mackay IR, Vaillant F, Wang ZX, Hertzog PJ. 1992. Validation of the Mtt Dye Assay for Enumeration of Cells in Proliferative and Antiproliferative Assays. Biochemistry International 27:501-510.

Maurer T, Muller SP, Kraushaar-Czarnetzki B. 2001. Aggregation and peptization behavior of zeolite crystals in sols and suspensions. Industrial & Engineering Chemistry Research 40:2573-2579.

Mintova S, Olson NH, Bein T. 1999a. Electron microscopy reveals the nucleation mechanism of zeolite Y from precursor colloids. Angewandte Chemie-International Edition 38:3201-3204.

Mintova S, Olson NH, Valtchev V, Bein T. 1999b. Mechanism of zeolite a nanocrystal growth from colloids at room temperature. Science 283:958-960.

Napierska D, Thomassen LCJ, Rabolli V, Lison D, Gonzalez L, Kirsch-Volders M, Martens JA, Hoet PH. 2009. Size-Dependent Cytotoxicity of Monodisperse Silica Nanoparticles in Human Endothelial Cells. Small 5:846-853.

Napierska D, Thomassen LCJ, Lison D, Martens JA, Hoet PH. 2010. The nanosilica hazard: another variable entity. Particle and Fibre Toxicology 7.

Nikolakis V. 2005. Understanding interactions in zeolite colloidal suspensions: A review. Current Opinion in Colloid & Interface Science 10:203-210.

Ndiege N, Raidoo R, Schultz MK, Larsen S. 2011. Preparation of a Versatile Bifunctional Zeolite for Targeted Imaging Applications. Langmuir 27:2904-2909.

Oberdorster G. 2000. Toxicology of ultrafine particles: in vivo studies. Philosophical Transactions of the Royal Society of London Series A-Mathematical Physical and Engineering Sciences 358:2719-2739.

Oberdorster G, Oberdorster E, Oberdorster J. 2005. Nanotoxicology: An emerging discipline evolving from studies of ultrafine particles. Environmental Health Perspectives 113:823-839.

Pearce ME, Mai HQ, Lee N, Larsen SC, Salem AK. 2008. Silicalite nanoparticles that promote transgene expression. Nanotechnology 19.

Petushkov A, Intra J, Graham JB, Larsen SC, Salem AK. 2009. Effect of Crystal Size and Surface Functionalization on the Cytotoxicity of Silicalite-1 Nanoparticles. Chemical Research in Toxicology 22:1359-1368.

Petushkov A, Freeman J, Larsen SC. 2010a. Framework Stability of Nanocrystalline NaY in Aqueous Solution at Varying pH. Langmuir 26:6695-6701.

Petushkov, A., N. Ndiege, A. K. Salem, and S. C. Larsen, 2010b, Toxicity of Silica Nanomaterials: Zeolites, Mesoporous Silica, and Amorphous Silica Nanoparticles, in JC Fishbein ed., Advances in Molecular Toxicology: Elsevier, p. 223.

Rabolli V, Thomassen LCJ, Princen C, Napierska D, Gonzalez L, Kirsch-Volders M, Hoet PH, Huaux F, Kirschhock CEA, Martens JA *et al.* 2010. Influence of size, surface area and microporosity on the in vitro cytotoxic activity of amorphous silica nanoparticles in different cell types. Nanotoxicology 4:307-318.

Schoeman BJ, Sterte J, Otterstedt JE. 1994. Colloidal Zeolite Suspensions. Zeolites 14:110-116.

Seaton A, Tran L, Aitken R, Donaldson K. 2010. Nanoparticles, human health hazard and regulation. Journal of the Royal Society Interface 7:S119-S129.

Singh S, Shi TM, Duffin R, Albrecht C, van Berlo D, Hoehr D, Fubini B, Martra G, Fenoglio I, Borm PJA *et al.* 2007. Endocytosis, oxidative stress and IL-8 expression in human lung epithelial cells upon treatment with fine and ultrafine TiO2: Role of the specific surface area and of surface methylation of the particles. Toxicology and Applied Pharmacology 222:141-151.

Slowing II, Wu CW, Vivero-Escoto JL, Lin VSY. 2009. Mesoporous Silica Nanoparticles for Reducing Hemolytic Activity Towards Mammalian Red Blood Cells. Small 5:57-62.

Stern ST, Mcneil SE. 2008. Nanotechnology safety concerns revisited. Toxicological Sciences 101:4-21.

Stoeger T, Takenaka S, Frankenberger B, Ritter B, Karg E, Maier K, Schulz H, Schmid O. 2009. Deducing in Vivo Toxicity of Combustion-Derived Nanoparticles from a Cell-Free Oxidative Potency Assay and Metabolic Activation of Organic Compounds. Environmental Health Perspectives 117:54-60.

Stone V, Johnston H, Schins RPF. 2009. Development of in vitro systems for nanotoxicology: methodological considerations. Critical Reviews in Toxicology 39:613-626.

Suh WH, Suslick KS, Stucky GD, Suh YH. 2009. Nanotechnology, nanotoxicology, and neuroscience. Progress in Neurobiology 87:133-170.

Thomassen LCJ, Aerts A, Rabolli V, Lison D, Gonzalez L, Kirsch-Volders M, Napierska D, Hoet PH, Kirschhock CEA, Martens JA. 2010. Synthesis and Characterization of Stable Monodisperse Silica Nanoparticle Sols for in Vitro Cytotoxicity Testing. Langmuir 26:328-335.

Tosheva L, Valtchev VP. 2005. Nanozeolites: Synthesis, crystallization mechanism, and applications. Chemistry of Materials 17:2494-2513.

Tsotsalas M, Busby M, Gianolio E, Aime S, De Cola L. 2008. Functionalized nanocontainers as dual magnetic and optical probes for molecular imaging applications. Chemistry of Materials 20:5888-5893.

Tsotsalas MM, Kopka K, Luppi G, Wagner S, Law MP, Schafers M, De Cola L. 2010. Encapsulating In-111 in Nanocontainers for Scintigraphic Imaging: Synthesis, Characterization, and In Vivo Biodistribution. Acs Nano 4:342-348.

Vassault, A., 1983, Methods of Enzymatic Analysis, in MO Bergmeyer ed., Methods of Enzymatic Analyses: Weinheim, Germany, Wiley VCH, p. 118-126.

Vermeiren W, Gilson JP. 2009. Impact of Zeolites on the Petroleum and Petrochemical Industry. Topics in Catalysis 52:1131-1161.

Warheit DB. 2008. How meaningful are the results of nanotoxicity studies in the absence of adequate material characterization? Toxicological Sciences 101:183-185.

Worle-Knirsch JM, Pulskamp K, Krug HF. 2006. Oops they did it again! Carbon nanotubes hoax scientists in viability assays. Nano Letters 6:1261-1268.

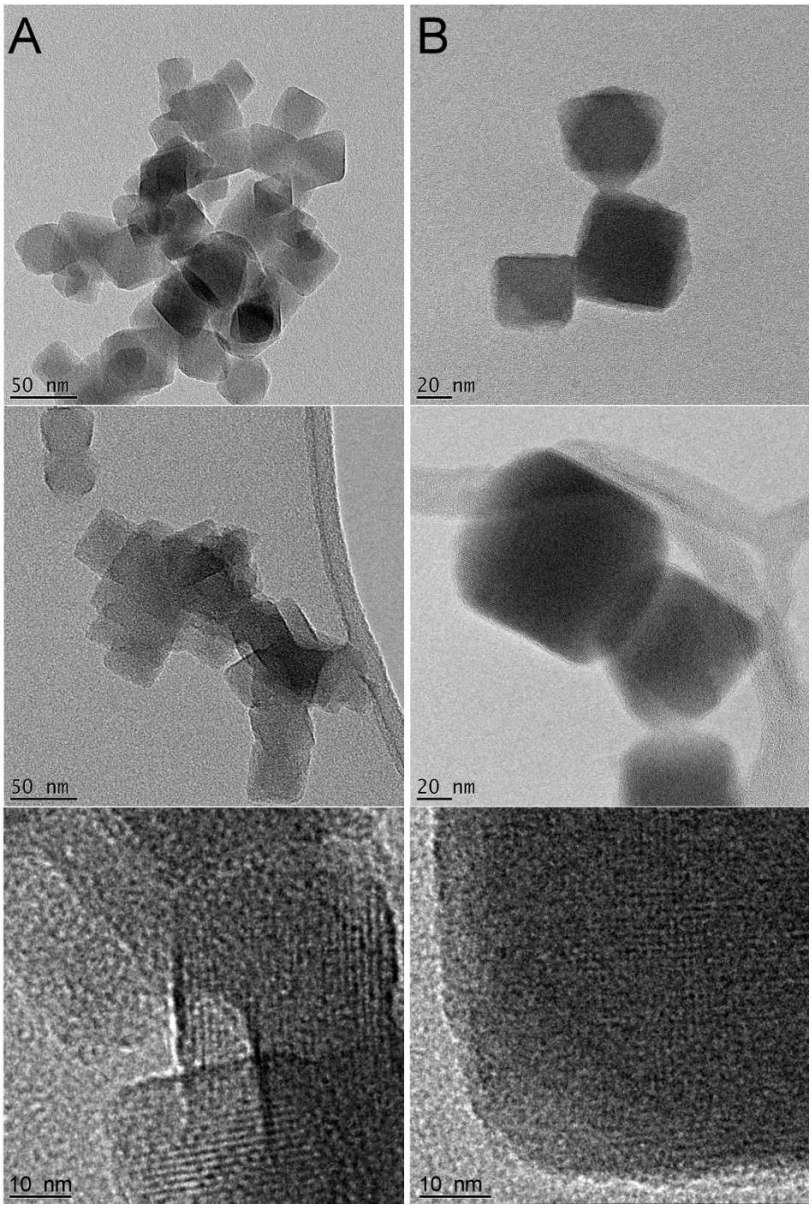

Figure 1: TEM pictures of zeolite Y (column A) and zeolite A (column B) reveal size, morphology and lattice fringes of the nanocrystals.

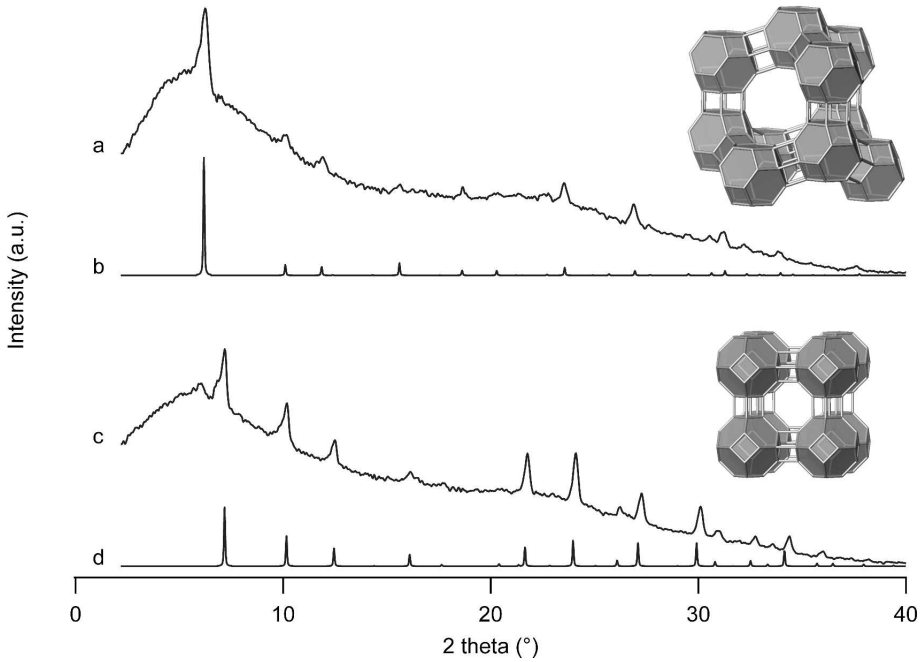

Figure 2: XRD pattern of nanozeolite Y (a), micron size zeolite Y (b), nanozeolite A (c) and micron size zeolite A (d). XRD patterns of micron size zeolites are duplicated from Baerlocher et al. (2007).

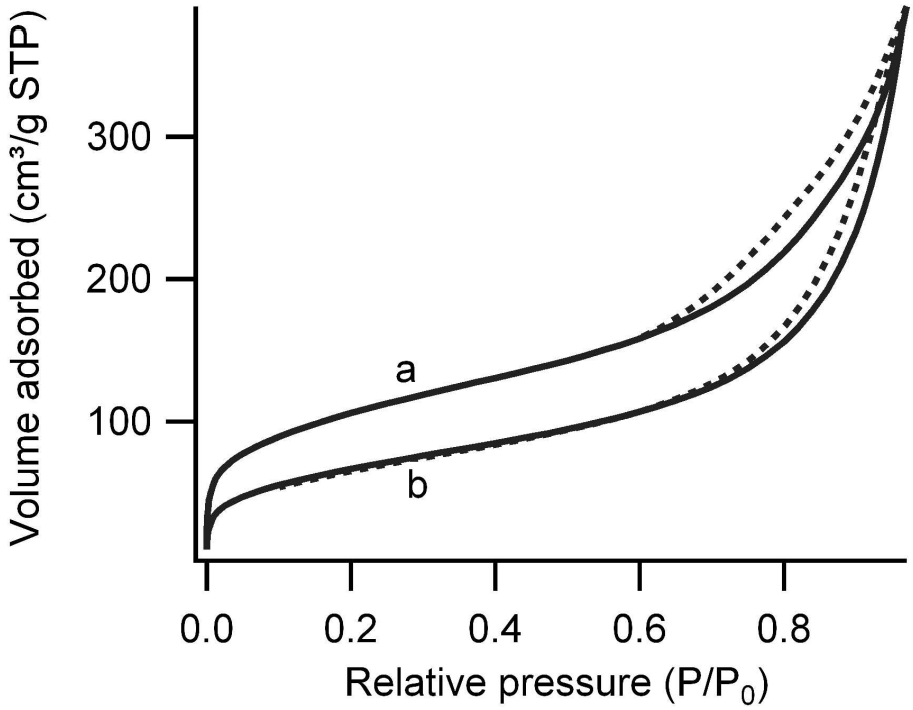

Figure 3: Nitrogen sorption isotherm of zeolite Y (a) and zeolite A (b). The ad- and desorption branches are in full and dotted lines, respectively.

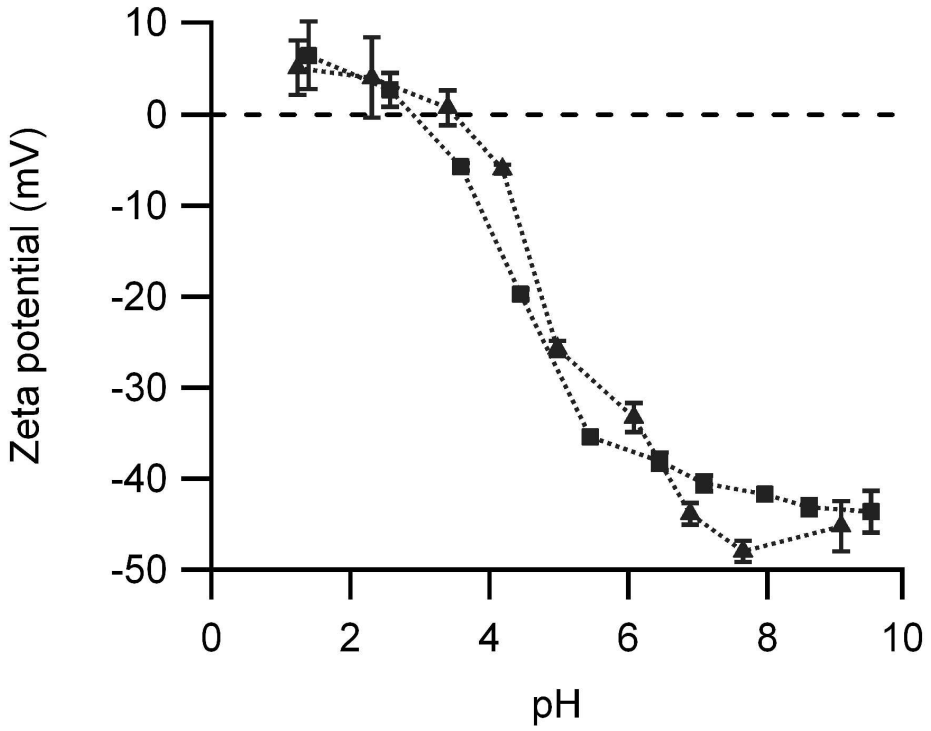

Figure 4: Zeta potential of nanozeolite Y (squares) and nanozeolite A (triangles) in water as a function of pH.

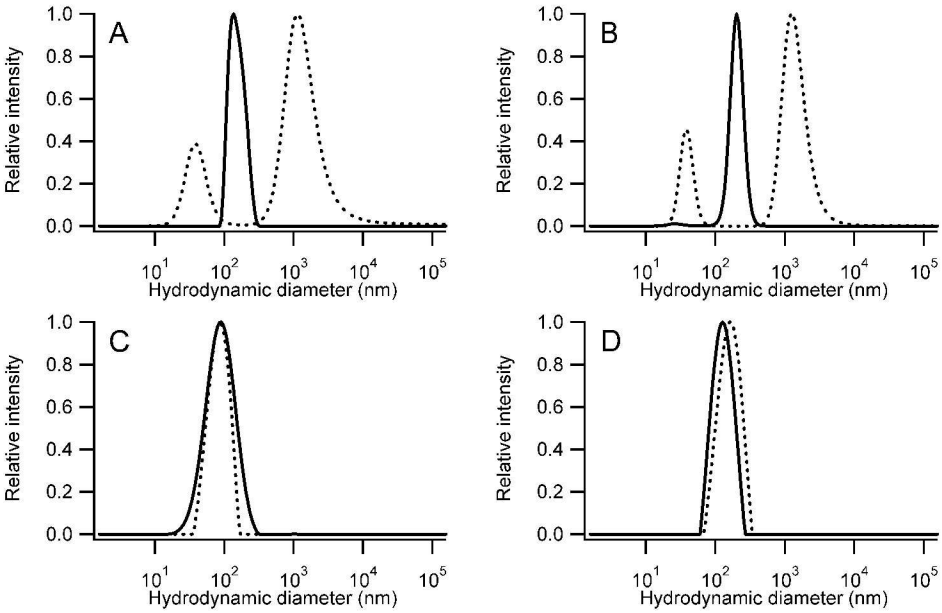

Figure 5: Evolution of hydrodynamic diameter of 25 µg/ml nanozeolites after 0 h (full line) and 24 h (dotted line) incubation in cell culture medium: (A) zeolite Y in DMEM-, (B) zeolite A in DMEM-, (C) zeolite Y in DMEM+, (D) zeolite A in DMEM+.

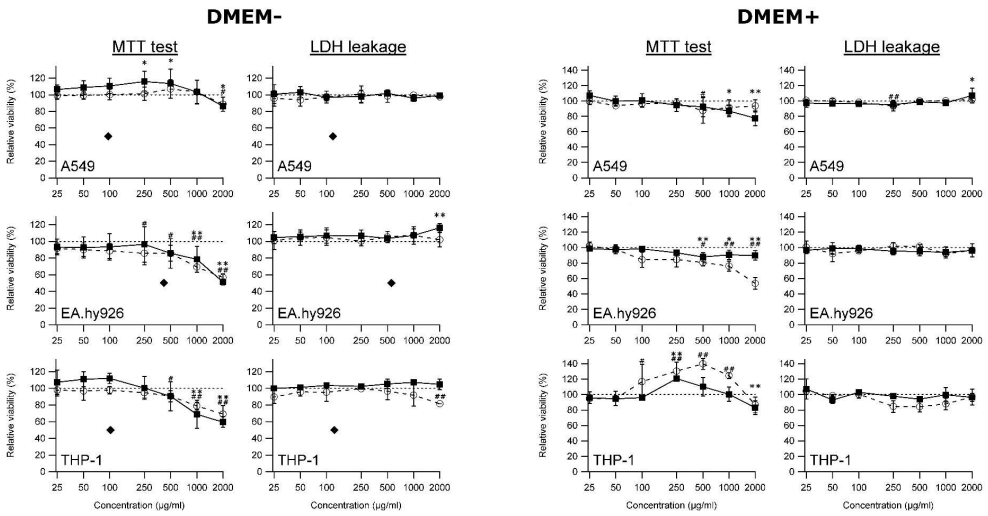

Figure 6: Dose-effect relationships in epithelial cells (A549, top), endothelial cells (EA.hy926, middle) and macrophages (THP-1, bottom) after 24 h exposure to the zeolite Y (full squares) and zeolite A (open circles) nanocrystals. Cells were exposed to nanozeolites in DMEM in absence of FCS (DMEM-: left pane) or presence of 2% FCS (DMEM+: right panel). Viability was assessed with MTT test (left column) and LDH leakage determination (right column) and results are presented as a percentage of the control values (average ± SD, n ≥ 6). The EC50 of the positive control, amorphous silica of 60 nm, in DMEM- is displayed in each graph by a diamond marker. Differences among means were considered significant with *p<0.05, and **p<0.01 for responses to nanozeolite Y and #p<0.05, and ##p<0.01 for responses to nanozeolite A.

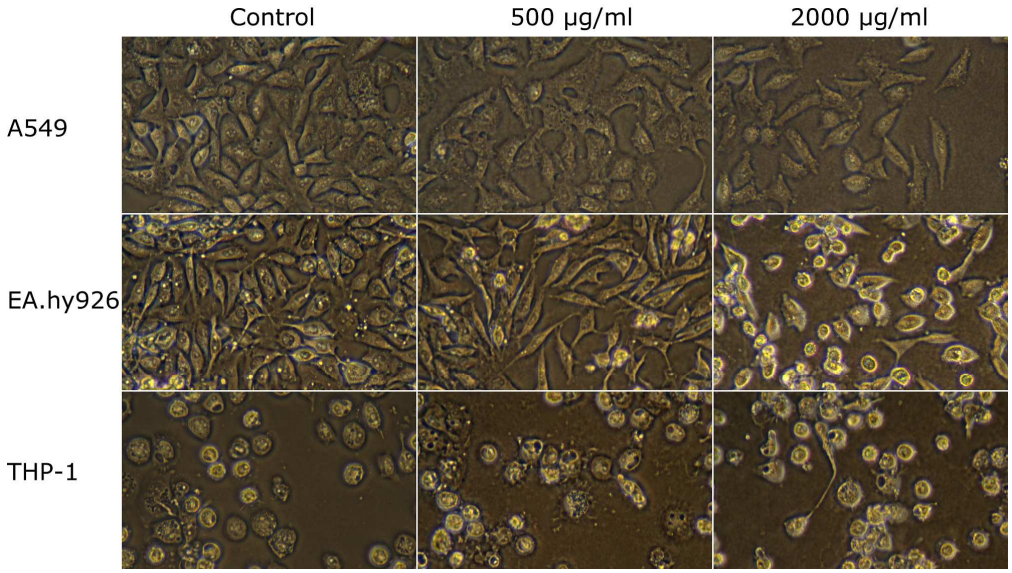

Figure 7: Light microscopy images of control cells and cells exposed to 500 µg/ml and 2000 µg/ml of zeolite Y after 24h exposure in DMEM-.

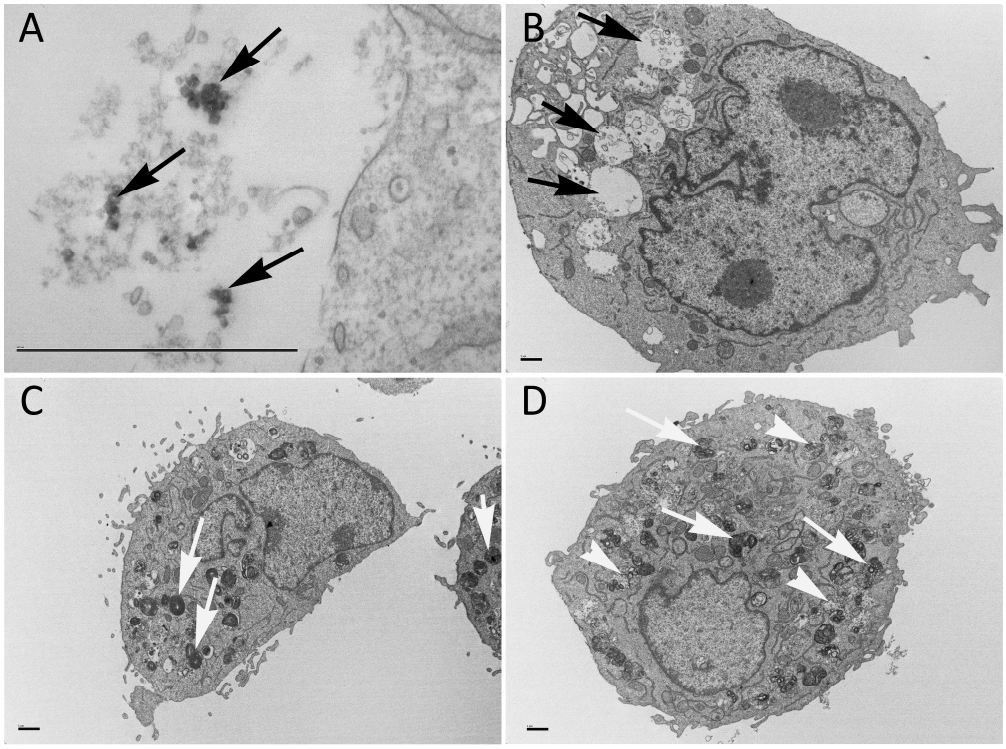

Figure 8: Electron micrographs of cells exposed to 250 μg/ml zeolites for 24 h. (A) A few particles of zeolite Y (black arrows) are evident within a vacuole of a THP-1 cell exposed in the absence of FCS. (B) Similar vacuoles (black arrows) are present in THP-1 cells exposed to this zeolite in the presence of FCS. (C) A549 cells exhibit very few vacuoles but, like controls, numerous lamellar bodies (white arrows) are present. (D) EA.hy926 cells resemble controls, with several lamellar bodies (white arrows) and multivesicular bodies (white arrowheads). Scale bars = 1μm.
168x125mm (600 x 600 DPI)